Inorganic Chemistry

Article

pubs.acs.org/IC

Monodispersed Ag Nanoparticles as Catalyst: Preparation Based on Crystalline Supramolecular Hybrid of Decamethylcucurbit[5]uril and Silver Ions

Hong-Fang Li, Jian Lü, Jing-Xiang Lin, and Rong Cao*

State Key Laboratory of Structural Chemistry, Fujian Institute of Research on the Structure of Matter, Chinese Academy of Sciences, Fuzhou, Fujian 350002, People's Republic of China

Supporting Information

ABSTRACT: Monodispersed silver nanoparticles (Ag^0 NPs) have been first prepared on the basis of a postsynthesis via mild reduction from a new crystalline supramolecular hybrid solid assembled from Ag^+ ions and decamethylcucurbit[5]uril ($Me_{10}CB[5]$). Uniform growth of nearly spherical Ag^0 NPs with an average size of ca. 4.4 nm was observed on the organic $Me_{10}CB[5]$ support to form **Ag@Me$_{10}$CB[5]** composite material. The as-synthesized composite material was characterized by a range of physical measurements (PXRD, TGA, XPS, ICP, TEM, etc.) and was further exploited as a heterogeneous catalyst for the reduction of various nitrophenols in the presence of $NaBH_4$. The kinetics of the reduction process was monitored under various experimental conditions. The **Ag@Me$_{10}$CB[5]** composite material showed excellent catalytic performance over the reduction reactions and remained active after several consecutive cycles.

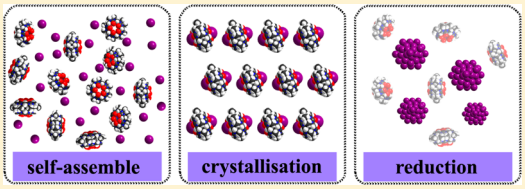

INTRODUCTION

Metal nanoparticles (NPs) have been an attractive subject of research in the realm of nanoscience and technology, owing to features distinct from those of their bulk counterparts. Research attention has thus been focused on the preparation and characterization of metal NPs in terms of both fundamental and practical research.[1,2] Among the various metal NPs, silver (Ag^0) NPs have received significant attention, because of their extraordinary properties suitable for applications in antibacterial, anti-inflammatory, antiviral, wound healing, and catalysis.[3,4]

Cucurbit[*n*]urils (CB[*n*]s) are a family of barrel-shaped macrocyclic molecules featuring a hydrophobic cavity with two identical carbonyl-fringed portals.[5] Because of their unique structures and outstanding multiple recognition locations, CB[*n*]s have been widely studied in coordination and supramolecular chemistry, as well as host−guest recognition.[6] The combination of the concepts of synthetic chemistry and materials science, applying CB[*n*] molecules to the fabrication of metal NPs, offers great opportunities to produce unique organic−inorganic composite materials. In recent years, phenomenal progress has been achieved in using CB[*n*]s as precursors to prepare metal NPs (especially Au^0 and Ag^0 NPs).[7−10] In 2007, García et al. reported the stabilization of Au^0 NPs with CB[*n*]s upon tetrachloroauric acid reduction using sodium borohydride.[7] A series of subsequent studies targeted at Au^0 NP preparation in the presence of CB[*n*]s were carried out.[8] By means of a similar method, Ag^0 NPs could be prepared upon reduction of silver nitrate with sodium borohydride and sodium hydroxide in the presence of CB[8] or CB[7], respectively.[9] Nevertheless, the as-prepared metal NPs were dispersed in solution and could hardly be separated as solid materials by a facile method; thus applications, for example as catalysts, were greatly limited. It was not until very recently that successful syntheses of Pd^0 and Pt^0 NPs as catalysts were reported by Cao's group.[10] In these cases, palladium and platinum chloride were treated with sodium borohydride in the presence of CB[6] and the as-prepared composite material catalysts exhibited excellent catalytic activity, stability, and reusability. However, fine control of the morphology and particle size of the as-prepared metal NPs was somewhat difficult. In the reported synthetic strategy of metal NPs in the presence of CB[*n*]s, strong reduction agents, e.g. sodium borohydride, were generally included, which easily led to the growth of large metal particles and particle aggregations (especially for the systems of Au^0 and Ag^0 NPs). Therefore, exploring a simple and mild synthetic method for the preparation of metal NPs with manageable morphology and size favored by CB[*n*]s has great theoretical and practical significance.

Herein, we report the preparation of well-dispersed Ag^0 NPs supported on decamethylcucurbit[5]uril ($Me_{10}CB[5]$) via a green and facile postsynthetic method from the crystalline supramolecular hybrid of $Me_{10}CB[5]$ and Ag^+ ions ($\{[Ag(H_2O)]_2(H_2O@Me_{10}CB[5])\}\cdot 2NO_3\cdot 2H_2O$, complex **1**). Complex **1** is, to the best of our knowledge, the first example of a crystalline supramolecular hybrid solid based solely on noble metal ions and CB[*n*], without secondary structure inducers. By means of mild thermal treatment of complex **1** precursors under an H_2 atmosphere, spherical Ag^0 NPs with a average size of ca. 4.4 nm were produced in situ and grew on the organic $Me_{10}CB[5]$ support to form **Ag@Me$_{10}$CB[5]** composite

Received: February 27, 2014
Published: May 12, 2014

dx.doi.org/10.1021/ic500464v | Inorg. Chem. 2014, 53, 5692−5697

material. The as-prepared **Ag@Me$_{10}$CB[5]** composite material exhibited excellent catalytic activity and reusability in the reduction reactions of various nitrophenols.

EXPERIMENTAL SECTION

General Considerations. All chemicals were commercially purchased and used without purification. Me$_{10}$CB[5] was synthesized according to the reported process.[11] Elemental analyses (C, H, and N) were carried on an Elementar Vario EL III analyzer. Ag loading was determined with a Jobin Yvon Ultima 2 inductively coupled plasma emission spectrometer (ICP). Powder X-ray diffractions (PXRD) were carried out with a Rigaku DMAX 2500 diffractometer. Thermogravimetric analysis (TGA) was performed under a flow of nitrogen by using a TA SDT-Q600 instrument. X-ray photoelectron spectra (XPS) were collected at a takeoff angle of 45° using a PHI Quantum 2000 scanning ESCA microprobe (Physical Electronics, USA) with an Al Kα X-ray line (1486.6 eV). Transmission electron microscope (TEM) images were taken on an FEI TECNAI G2 F20 microscope at an accelerating voltage of 200 kV. The **Ag@Me$_{10}$CB[5]** composite material was ultrasonically dispersed in ethanol and deposited on the holey carbon film on a copper grid prior to the TEM observation.

Synthesis of Ag@Me$_{10}$CB[5] Composite Material. The crystalline supramolecular hybrid $\{[Ag(H_2O)]_2(H_2O@Me_{10}CB[5])\}\cdot 2NO_3\cdot 2H_2O$ (complex **1**) was synthesized and used as a precursor to produce **Ag@Me$_{10}$CB[5]** composite material. In a typical recipe, $AgNO_3$ (1.6 g, 10 mmol) and Me$_{10}$CB[5] (0.97 g, 1 mmol) were dissolved in 75 mL of ultrapure water with magnetic stirring. The resulting white precipitate was removed by filtration, and the mother liquor was placed at room temperature for several days in the dark. Colorless crystals of complex **1** (0.53 g, 37.8% yield based on Me$_{10}$CB[5]) were collected by filtration and dried in air. Anal. Calcd for $C_{40}H_{60}N_{22}O_{21}Ag_2$: C, 34.3; H, 4.32; N, 22.0. Found: C, 34.6; H, 4.38; N, 22.0. The hybrid solid precursor was then transferred to a tubular furnace and heated to 200 °C for 4 h under an H_2 atmosphere. **Ag@Me$_{10}$CB[5]** composite material was readily produced through in situ reduction of the precursor complex **1**. The overall synthetic procedure of the composite material is illustrated in Scheme 1.

Scheme 1. Proposed Synthetic Route of the Composite Material Ag@Me$_{10}$CB[5]

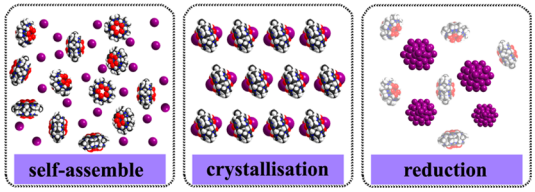

X-ray Crystallography. Single-crystal X-ray diffraction data of complex **1** were collected on a Rigaku Saturn 70 (4 × 4 bin mode) diffractometer equipped with graphite-monochromated Mo Kα radiation (λ = 0.71073 Å) and a CCD area detector. Empirical absorption corrections were applied to the data using the Crystal Clear program.[12] Structural solutions and full matrix least-squares refinements based on F^2 were performed with the SHELXS-97 and SHELXL-97 program packages, respectively.[13] All of the non-hydrogen atoms were refined anisotropically. Hydrogen atoms on the disassociated water molecules (O2W and O3W) were not located from a difference Fourier map or by theoretical methods, due to the limited quality of the crystal data. Crystal data and structure refinement parameters are given in Table S1 (Supporting Information). CCDC-971702 contains supplementary crystallographic data for this paper. These data can be obtained free of charge from The Cambridge Crystallographic Data Centre via www.ccdc.cam.ac.uk/data_request/cif.

Catalytic Experiments. The catalytic activity of the composite material **Ag@Me$_{10}$CB[5]** was investigated in reduction reactions of *n*-nitrophenols (*n*-NP, *n* = 4–2) to the corresponding *n*-aminophenols (*n*-AP) in the presence of sodium borohydride. For a standard procedure, a certain amount (3.75×10^{-4} mmol, 0.7 mg) of **Ag@Me$_{10}$CB[5]** composite was added to the reaction mixture of *n*-NP (15 mL, 0.01 M), water (100 mL), and $NaBH_4$ (1.5 mL, 1 M) solution at 25 °C. The evolution of the absorption spectra due to the reduction of *n*-NP to *n*-AP was recorded using a UV2550 UV–visible (UV–vis) spectrophotometer. UV–vis spectra of blank reactions without catalysts were also recorded as references. The reusability of the catalyst was studied by separating the **Ag@Me$_{10}$CB[5]** composite from the solution after each cycle of the reaction, washing with water, drying in air, and reusing for the next run.

RESULTS AND DISCUSSION

Characterization of the Crystalline Hybrid Precursor Complex 1. The crystalline hybrid solid $\{[Ag(H_2O)]_2(H_2O@Me_{10}CB[5])\}\cdot 2NO_3\cdot 2H_2O$ (complex **1**) was synthesized from an aqueous solution of Me$_{10}$CB[5] and $AgNO_3$. The crystal structure of complex **1** was confirmed by the combination use of single-crystal X-ray diffraction, elemental analysis, and thermal gravimetric analyses. In the structure of complex **1**, two Ag^+ cations are capped to the portals of a Me$_{10}$CB[5] unit through the coordination of three carbonyl oxygen atoms and one aqua ligand to a Ag^+, giving rise to a "half-open" molecular capsule (Figure 1). One water molecule is encapsulated inside

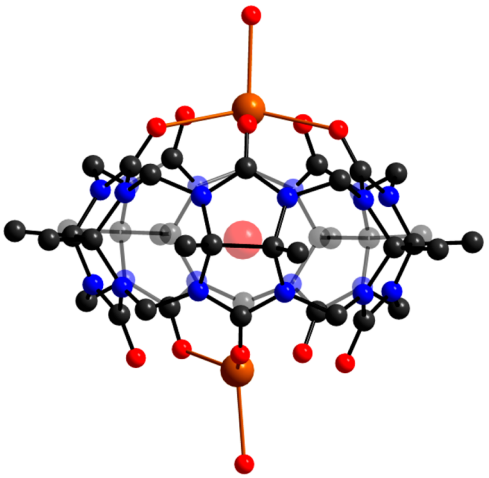

Figure 1. View of the "half-open" molecular capsule of Me$_{10}$CB[5] and Ag^+ cations in complex **1**.

the cavity of a molecular capsule. Moreover, two uncoordinated water molecules and two NO_3^- anions, which play the role of charge balancing, appear in the crystal lattice. Adjacent molecular capsules are interconnected through the hydrogen bonds (H-bonds) among the aqua ligand, portal carbonyl oxygen atoms, and uncoordinated water molecules (H-bond distances 2.986 and 2.990 Å, respectively), giving rise to a one-dimensional (1D) supramolecular chain structure (Figure 2). NO_3^- anions are anchored on each side of the supramolecular chain through weak H-bond interactions (H-bond distance 3.355 Å) (Figure 2). It is well-known that the portal carbonyl groups of CB[*n*] are capable of coordinating with alkali metals, alkaline-earth metals, and lanthanide ions.[14] Transition-metal ions normally form hydrates or complex fragments and interact with CB[*n*] through H-bonding interactions.[14a] Only a few exceptions in which transition-metal ions attach to the portal carbonyl groups of CB[*n*] via coordinative bonds have been documented, even though extra transition-metal complex moieties were observed in the crystal lattice as structure

dx.doi.org/10.1021/ic500464v | Inorg. Chem. 2014, 53, 5692–5697

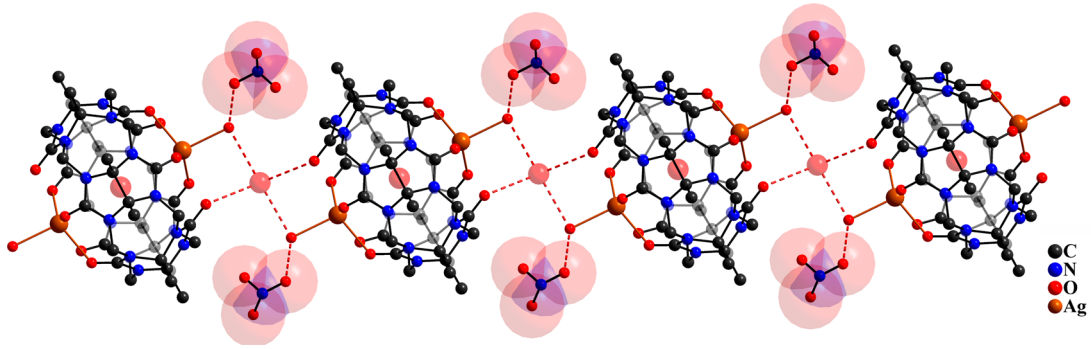

Figure 2. View of the 1D supramolecular chain structure in complex **1**.

inducers.[15] To the best of our knowledge, complex **1** represents the first example of a crystalline supramolecular hybrid solid based solely on noble-metal ions and CB[*n*].

The phase purity and homogeneity of the crystalline hybrid precursor complex **1** were identified by powder X-ray diffraction (PXRD) at room temperature (Figure 3). The

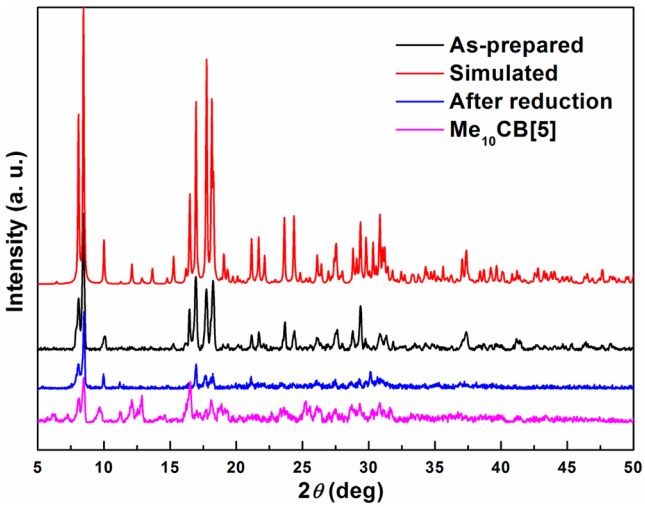

Figure 3. Simulated and experimental PXRD patterns of the complex **1** (red and black, respectively), the reduced composite material **Ag@Me$_{10}$CB[5]** (blue), and the pure organic support Me$_{10}$CB[5] (purple).

experimental PXRD pattern and that simulated from single-crystal X-ray diffraction data of complex **1** are nearly identical, which clearly indicates the good purity and homogeneity of the complex precursor. Thermogravimetric analysis (TGA) of the hybrid precursor complex **1** was recorded in the temperature range 20−900 °C to reveal the thermal stability as well as to determine the water molecules present. The TGA curve shows continuous weight loss before 200 °C (Figure S1, Supporting Information), corresponding to the release of uncoordinated and coordinated water molecules (five water molecules per formula unit; calcd 6.4%, found 6.6%). A plateau is observed between 200 and 300 °C, followed by further decomposition of the material. A rational reduction temperature of 200 °C to postsynthesize the composite material **Ag@Me$_{10}$CB[5]** was optimized, which ensured the complete reduction of Ag^+ ions into Ag^0 NPs without destruction of the Me$_{10}$CB[5] organic support.

Characterization of the Composite Material Ag@Me$_{10}$CB[5]. Upon postsynthetic reduction by thermal treatment at 200 °C for 4 h under a H_2 atmosphere, the colorless crystalline bulky compound became gray, indicating a phase change of the sample. The TGA curve of the postsynthesized composite material **Ag@Me$_{10}$CB[5]** shows continuous weight loss before 300 °C (Figure S1, Supporting Information), corresponding to the release of adsorbed water. The organic support of the composite began to decompose at lower temperature in comparison with the original complex **1** due to the weaker interaction between Ag NPs and the Me$_{10}$CB[5] support. The PXRD pattern of the **Ag@Me$_{10}$CB[5]** composite matches fairly well with the PXRD of the pure Me$_{10}$CB[5] sample, which confirms the major content of the organic support. Characteristics of the Ag^0 NPs were missing from the PXRD pattern, presumably due to the weak diffraction intensity of Ag^0 NPs in comparison with that of the Me$_{10}$CB[5] support (Figure 3). However, direct evidence for the formation of metallic Ag^0 was provided by XPS measurements (Figure 4).

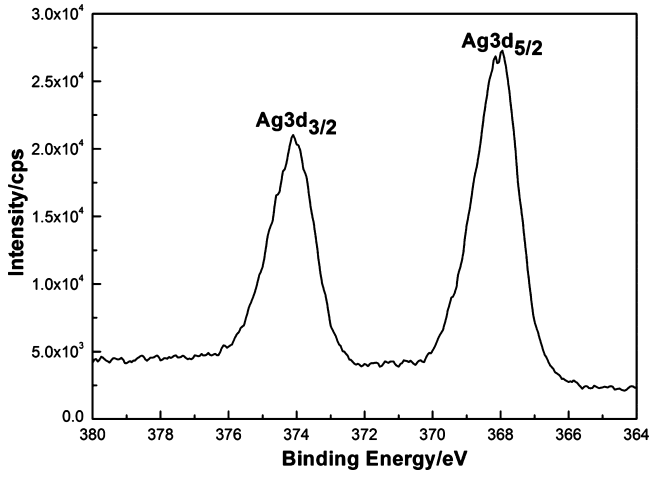

Figure 4. XPS spectra of the composite material **Ag@Me$_{10}$CB[5]**, indicating the presence of Ag^0 species.

The Ag species exhibited two characteristic peaks with binding energies of 368.1 and 374.1 eV due to the $3d_{5/2}$ and $3d_{3/2}$ electrons of Ag^0, respectively. These peaks suggested the successful in situ formation of Ag^0 NPs from the postsynthetic reduction of the crystalline supramolecular hybrid precursor. The ICP result showed that the loading content of Ag^0 NPs was 11.6 wt %. The morphology and particle size of Ag^0 NPs in the composite material **Ag@Me$_{10}$CB[5]** were studied directly from TEM images. As shown in Figure 5, monodispersed spherical Ag^0 NPs with a diameter of ca. 4.4 nm have grown on site on the Me$_{10}$CB[5] support. A high-resolution TEM image

dx.doi.org/10.1021/ic500464v | Inorg. Chem. 2014, 53, 5692−5697

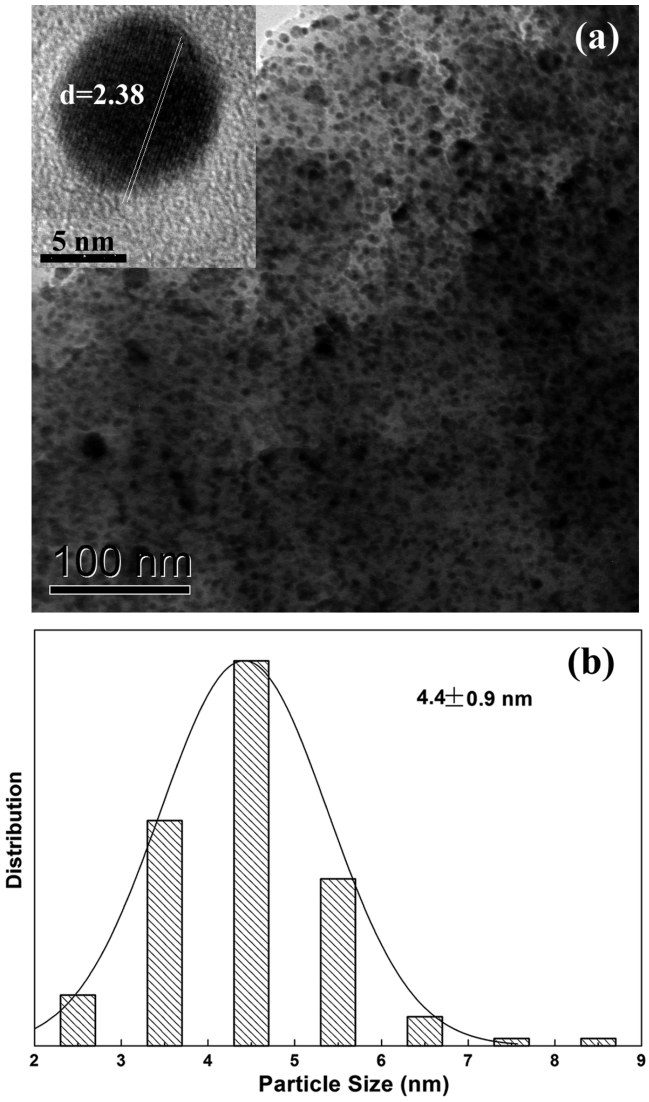

Figure 5. TEM micrograph (a) and size distribution (b) of the composite material **Ag@Me$_{10}$CB[5]**, showing Ag^0 NPs supported on Me$_{10}$CB[5].

(HRTEM, Figure 5a inset) indicates that the Ag^0 NPs are highly crystalline with a plane distance of 2.38 Å, which corresponds to the [111] lattice plane of Ag^0 NPs. Me$_{10}$CB[5] plays an important role in stabilizing Ag NPs. The Ag NPs aggregated severely to form large particles when the Me$_{10}$CB-[5] support was removed (Figure S2, Supporting Information).

Catalytic Performance in Organic Reduction Reactions. The nitrophenols are among the most common organic pollutants in industrial and agricultural wastewater. However, aminophenols are important intermediates for the manufacture of analgesic and antipyretic drugs.[16] In this context, the reduction of nitrophenols to aminophenols becomes much more fascinating for pollution abatement as well as industrial applications. The reduction reaction of 4-nitrophenol (4-NP) in the presence of NaBH$_4$ at 25 °C was selected as a model system to demonstrate the catalytic performance of the composite material **Ag@Me$_{10}$CB[5]**. Specifically, the catalytic reduction of nitrophenols with NaBH$_4$ was spectrophotometrically performed using **Ag@Me$_{10}$CB[5]** as a catalyst in aqueous medium. A maximum absorption (λ_{max}) at ca. 317 nm was observed for the aqueous solution of 4-NP, as shown in Figure 6, which was red-shifted immediately to ca. 400 nm as a result of the formation of 4-nitrophenolate ions under alkaline

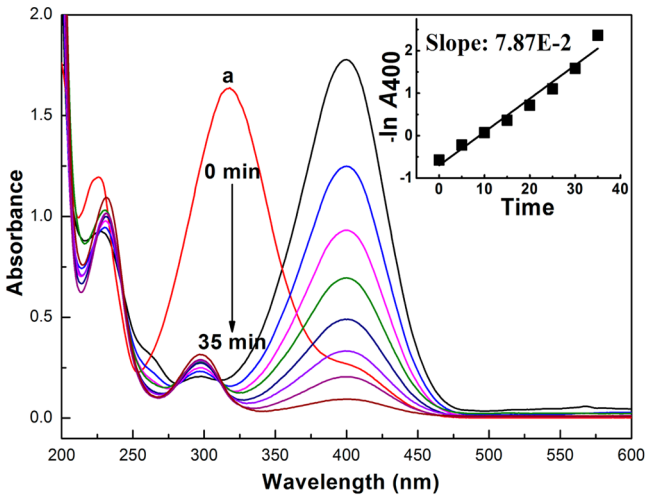

Figure 6. UV−vis spectral changes of characteristic bands of 4-NP in aqueous solution (red) and in the reduction reactions with composite material **Ag@Me$_{10}$CB[5]** as catalyst (multiple colors). Inset: corresponding pseudo-first-order plot of −ln A_{400} versus time.

conditions upon addition of a freshly prepared ice-cold aqueous solution of NaBH$_4$. In the absence of **Ag@Me$_{10}$CB[5]** catalyst, the characteristics at ca. 400 nm changed slightly with time (Figure S3, Supporting Information), suggesting an extremely slow process of the reduction reaction, which was in agreement with observations in previous reports.[17] Upon addition of **Ag@Me$_{10}$CB[5]** composite, the absorption peaks at ca. 400 nm decreased gradually with time and a new peak at 295 nm, characteristic of 4-AP, appeared alongside (Figure 6). During the catalytic reduction, the originally bright yellow solution became visually colorless after around 35 min, indicating completion of the reaction. Since NaBH$_4$ was used in excess, the reaction could be pseudo first order and the apparent rate constant was calculated by plotting −ln A_{400} vs time. The plot appeared nearly linear (Figure 6, inset), and the apparent rate constant value was calculated to be 7.87×10^{-2} min^{-1} with a normalized rate constant (k_{nor}) of 1.75 mmol^{-1} s^{-1}, which is comparable to a recent report of Au NPs with a k_{nor} value of 2.04 mmol^{-1} s^{-1}.[18] Furthermore, the catalytic reduction reaction of 4-NP was studied at different temperatures and the corresponding rate constants were calculated as given in Table 1 (entries 1−5). The activation energy was calculated to

Table 1. Rate Constant Values of the Reduction Reactions of *n*-NP in the Presence of Ag@Me$_{10}$CB[5] Catalyst

entry	substrate	T (°C)	k (min^{-1})	K_{nor} (mmol^{-1} s^{-1})
1	4-NP	10	0.0195	0.43
2	4-NP	25	0.0787	1.75
3	4-NP	40	0.172	3.82
4	4-NP	50	0.329	7.31
5	4-NP	60	0.635	14.1
6	2-NP	25	0.0535	1.19
7	3-NP	25	0.0111	0.25
8	2-CH$_3$-4-NP	25	0.0352	0.78
9	3-CH$_3$-4-NP	25	0.0288	0.64
10	2-Cl-4-NP	25	0.0454	1.01

dx.doi.org/10.1021/ic500464v | Inorg. Chem. 2014, 53, 5692−5697

be 53 kJ mol^{-1} by applying the Arrhenius equation to the kinetic data of entries 1−5 (Table 1 and Figure S4 (Supporting Information)).

For heterogeneous catalysis, the rate constant of the reaction generally increases linearly with the amount of catalyst.[19] These parameters have been determined for the current system. As shown in Figure 7, the rate constants are plotted against the

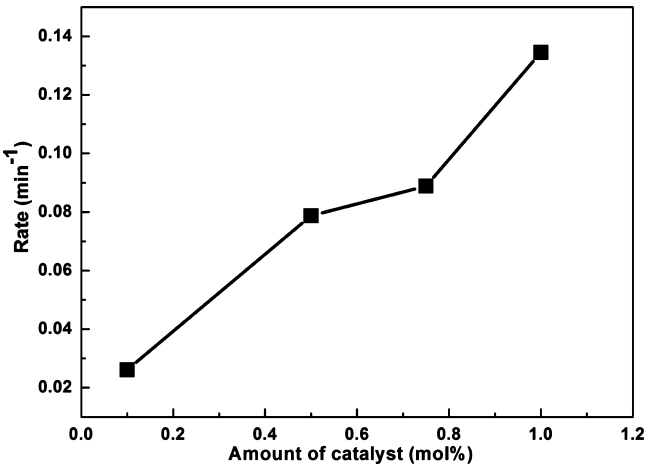

Figure 7. Plot of rate constants against the amount of **Ag@Me$_{10}$CB[5]** catalyst used for the reduction of 4-NP.

amount of catalyst used. In the current system, it has been found that the rate constant also increases with the increasing amount of **Ag@Me$_{10}$CB[5]** catalyst. The role of metal NPs is crucial in terms of electrochemical current potential in the reduction reactions.[20] In such reactions, electron transfer from BH_4^- to 4-NP occurs only when both are absorbed onto the surface of Ag^0 NPs. Thus, increasing the amount of **Ag@Me$_{10}$CB[5]** catalyst will provide a larger accessible substrate surface area for Ag^0 NPs, which in turn favors substrate adsorption and increases the rate constant.

In addition, the Ag^0 NP loaded composite material **Ag@Me$_{10}$CB[5]** is applicable to other nitrophenol reduction systems. As shown in Table 1 (entries 6−10), catalytic reductions with different reaction rates were successful with other nitrophenol precursors in the presence of **Ag@Me$_{10}$CB[5]** catalyst. It is well-known that 4- and 2-nitrophenolate ions are much more stable than 3-nitrophenolate ion.[21,22] For 4-nitrophenolate ion, the "negative" charge on oxygen is delocalized throughout the benzene ring (conjugation effect) and becomes resonance stabilized. For 2-nitrophenolate ion, the "negative" charge on oxygen is also delocalized throughout the benzene ring but not as effectively as in 4-nitrophenolate ion. For 3-nitrophenolate ion, however, there is no conjugation effect, only the -I effect (inductive effect) of the nitro group is valid. Moreover, the inductive effect of the nitro group is less effective due to steric hindrance and therefore it is less stable than other isomers. The rate of reduction of the nitrophenols is expected to follow the order 4-NP > 2-NP > 3-NP, which is in good agreement with the experimental results (Table 1). Moreover, the rate constants decrease greatly with the insertion of either electron-accepting (Cl) or -donating (CH_3) substituent groups in the ortho and meta positions of 4-NP due to the reduction of the conjugation effect.

Stability and reusability are important parameters for the practical applications of catalysts. The **Ag@Me$_{10}$CB[5]** catalyst has been tested for up to five consecutive cycles for the reduction reaction of 4-NP and monitored by UV−vis spectra. The calculated apparent rate constants, as plotted in Figure 8,

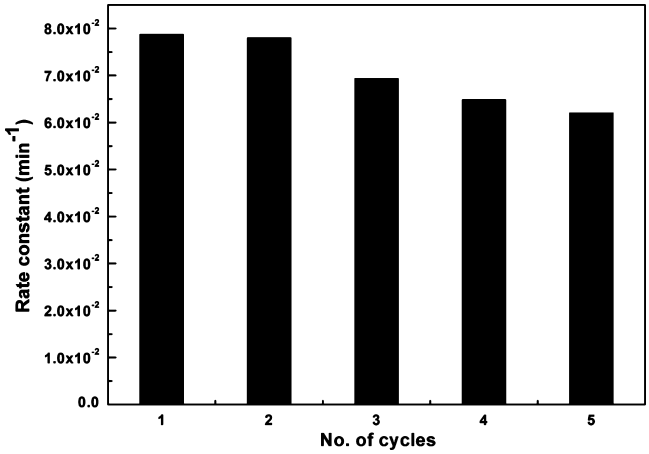

Figure 8. Rate constant values (k) of the catalytic reduction reaction of 4-NP in five consecutive cycles.

shows that the composite catalyst preserves more than 80% of the initial catalytic ability after it is recycled five times. The rational decrease of catalytic ability might account for the slight growth and aggregation of Ag^0 NPs on the $Me_{10}CB[5]$ support after several times of use, as confirmed by a TEM image (Figure S5, Supporting Information), as well as the insignificant loss of catalyst in the multiple separation processes.

CONCLUSION

In this work, a new crystalline supramolecular hybrid, $\{[Ag(H_2O)]_2(H_2O@Me_{10}CB[5])\}\cdot 2NO_3\cdot 2H_2O$ (complex **1**), was successfully synthesized from $Me_{10}CB[5]$ and Ag^+ ions as the first example of a crystalline solid based solely on noble-metal ions and CB[n]. Complex **1** was further used as a precursor for postsynthetic reduction under a H_2 atmosphere, which gave rise to a composite material (**Ag@Me$_{10}$CB[5]**) of monodispersed Ag^0 NPs with an average size of 4.4 nm supported on $Me_{10}CB[5]$. In comparison with the traditional reduction method for NP−CB[n] systems, we presented here a much greener and milder method, which prevented the growth of large Ag^0 NPs and particle aggregations. The morphology and the particle size of the as-prepared Ag^0 NPs were easily manageable. The **Ag@Me$_{10}$CB[5]** composite material was investigated as an efficient catalyst for the reduction of nitrophenols. Moreover, the **Ag@Me$_{10}$CB[5]** catalyst could be easily recycled several times, through simple centrifugation, without dramatic loss of catalytic activity. The **Ag@Me$_{10}$CB[5]** composite material, prepared through in situ reduction of the crystalline solid precursor (complex **1**), is promising as a catalyst for the conversion of nitro to amino compounds on a large scale.

ASSOCIATED CONTENT

Supporting Information

Figures, a table, and a CIF file giving TGA, UV−vis, TEM, and crystallographic data. This material is available free of charge via the Internet at http://pubs.acs.org.

dx.doi.org/10.1021/ic500464v | Inorg. Chem. 2014, 53, 5692−5697

AUTHOR INFORMATION

Corresponding Author

*E-mail for R.C.: rcao@fjirsm.ac.cn.

Notes

The authors declare no competing financial interest.

ACKNOWLEDGMENTS

We thank the 973 Program (2011CB932504 and 2012CB821705), NSFC (21331006, 21221001, 21101155 and 21203199), Fujian Key Laboratory of Nanomaterials (2006L2005), and the Key Project from CAS for financial support.

REFERENCES

(1) Katz, E.; Willner, I. *Angew. Chem.* **2004**, *116*, 6166−6235; *Angew. Chem., Int. Ed.* **2004**, *43*, 6042−6108.

(2) *Functional Nanomaterials*; Geckeler, K. E., Rosenberg, E., Eds.; American Scientific: Valencia, CA, USA, 2006.

(3) Wong, K. K. Y.; Liu, X. *Med. Chem. Commun.* **2010**, *1*, 125−131.

(4) Nair, L. S.; Laurencin, C. T. *J. Biomed. Nanotechnol.* **2007**, *3*, 301−316.

(5) (a) Rowan, A. E.; Elemans, J. A. A. W.; Nolte, R. J. M. *Acc. Chem. Res.* **1999**, *32*, 995−1006. (b) Lee, J. W.; Samal, S.; Selvapalam, N.; Kim, H.-J.; Kim, K. *Acc. Chem. Res.* **2003**, *36*, 621−63.

(6) (a) Lagona, J.; Mukhopadhyay, P.; Chakrabarti, S.; Isaacs, L. *Angew. Chem.* **2005**, *117*, 4922−4949; *Angew. Chem., Int. Ed.* **2005**, *44*, 4844−4870. (b) Gerasko, O. A.; Fedin, V. P. *Russ. J. Inorg. Chem.* **2011**, *56*, 2025−2046. (c) Suvitha, A.; Venkataramanan, N. S.; Mizuseki, H.; Kawa-zoe, Y.; Ohuchi, N. *J. Inclusion Phenom. Macrocyclic Chem.* **2010**, *66*, 213−218.

(7) Corma, A.; García, H.; Montes-Navajas, P.; Primo, A.; Calvino, J. J.; Trasobares, S. *Chem. Eur. J.* **2007**, *13*, 6359−6364.

(8) (a) Montes-Navajas, P.; Damonte, L. C.; García, H. *ChemPhysChem* **2009**, *10*, 812−816. (b) Montes-Navajas, P.; García, H. *J. Phys. Chem. C* **2010**, *114*, 18847−18852. (c) Lee, T.-C.; Scherman, O. A. *Chem. Commun.* **2010**, *46*, 2438−2440. (d) Taylor, R. W.; Lee, T. C.; Scherman, O. A.; Esteban, R.; Aizpupurua, J.; Huang, F. M.; Baumberg, J. J.; Mahajan, S. *ACS Nano* **2011**, *5*, 3878−3887. (e) Coulston, R. J.; Jones, S. T.; Lee, T.-C.; Appel, E. A.; Scherman, O. A. *Chem. Commun.* **2011**, *47*, 164−166. (f) Premkumar, T.; Geckeler, K. E. *Chem. Asian J.* **2010**, *5*, 2468−2476. (g) Lee, T.-C.; Scherman, O. A. *Chem. Eur. J.* **2012**, *18*, 1628−1633.

(9) (a) Lu, X.; Masson, E. *Langmuir* **2011**, *27*, 3051−3058. (b) Premkumar, T.; Lee, Y.; Geckeler, K. E. *Chem. Eur. J.* **2010**, *16*, 11563−11566.

(10) (a) Cao, M.; Wu, D.; Gao, S.; Cao, R. *Chem. Eur. J.* **2012**, *18*, 12978−12985. (b) Cao, M.; Lin, J.; Yang, H.; Cao, R. *Chem. Commun.* **2010**, *46*, 5088−5090. (c) Cao, M.; Wei, Y.; Gao, S.; Cao, R. *Catal. Sci. Technol.* **2012**, *2*, 156−163.

(11) Shih, N.-Y. *Diss. Abstr. Int., B* **1982**, *B42*, 4071.

(12) Sheldrick, G. M. *SADABS*; University of Göttingen, Göttingen, Germany, 1996.

(13) *SHELXTL, version 5.10*; Siemens Analytical X-ray Instruments, Madison, WI, 1994.

(14) (a) Lü, J.; Lin, J.-X.; Cao, M.-N.; Cao, R. *Coord. Chem. Rev.* **2013**, *257*, 1334−1356. (b) Ni, X.-L.; Xiao, X.; Cong, H.; Liang, L.-L.; Cheng, K.; Cheng, X.-J.; Ji, N.-N.; Zhu, Q.-J.; Xue, S.-F.; Tao, Z. *Chem. Soc. Rev.* **2013**, *42*, 9480−9508. (c) Masson, E.; Ling, X.; Joseph, R.; Kyeremeh-Mensah, L.; Lu, X. *RSC Adv.* **2012**, *2*, 1213−1247.

(15) (a) Liu, J. X.; Long, L. S.; Huang, R. B.; Zheng, L. S. *Cryst. Growth Des.* **2006**, *6*, 2611−2614. (b) Gerasko, O. A.; Mainicheva, E. A.; Naumova, M. I.; Neumaier, M.; Kappes, M. M.; Lebedkin, S.; Fenske, D.; Fedin, V. P. *Inorg. Chem.* **2008**, *47*, 8869−8880. (c) Zeng, J. P.; Zhang, S. M.; Zhang, Y. Q.; Tao, Z.; Zhu, Q. J.; Xue, S. F.; Wei, G. *Cryst. Growth Des.* **2010**, *10*, 4509−4515. (d) Zeng, J. P.; Cong, H.; Chen, K.; Xue, S. F.; Zhang, Y. Q.; Zhu, Q. J.; Liu, J. X.; Tao, Z. *Inorg. Chem.* **2011**, *50*, 6521−6525. (e) Feng, X.; Li, Z.-F.; Xue, S.-F.; Tao, Z.; Zhu, Q.-J.; Zhang, Y.-Q.; Liu, J.-X. *Inorg. Chem.* **2010**, *49*, 7638−7640.

(16) Dotzauer, D. M.; Dai, J. H.; Sun, L.; Bruening, M. L. *Nano Lett.* **2006**, *6*, 2268−2272.

(17) (a) Lu, Y.; Mei, Y.; Drechsler, M.; Ballauff, M. *Angew. Chem., Int. Ed.* **2006**, *45*, 813−816. (b) Mei, Y.; Sharma, G.; Lu, Y.; Drechsler, M.; Ballauff, M.; Irrgang, T.; Kempe, R. *Langmuir* **2005**, *21*, 12229−12234. (c) Hayakawa, K.; Yoshimura, T.; Esumi, K. *Langmuir* **2003**, *19*, 5517−5521. (d) Lu, Y.; Mei, Y.; Ballauff, M.; Drechsler, M. *J. Phys. Chem. B* **2006**, *110*, 3930−3937.

(18) Jana, D.; Dandapat, A.; De, G. *Langmuir* **2010**, *26*, 12177−12184.

(19) Spiro, M. In *Essays in Chemistry*; Bradley, J. N., Gillard, R. D., Hudson, R. F., Eds.; Acadamic Press: London, 1973; Vol.5, p 63.

(20) (a) Freund, P. L.; Spiro, M. *J. Phys. Chem. B* **1985**, *89*, 1074−1077. (b) Miller, D. S.; Bard, A. J.; Mclendon, G.; Ferguson, J. *J. Am. Chem. Soc.* **1981**, *103*, 5336−5341.

(21) Finar, I. L. *Organic Chemistry: Fundamental Principles*, 6th ed.; ELBA: 1973; Vol. *1*, p 702.

(22) Li, H.; Gao, S.; Zheng, Z.; Cao, R. *Catal. Sci. Technol.* **2011**, *1*, 1194−1201.